PHYSICAL REVIEW VOLUME 180, NUMBER 1 5 APRIL 1969

Lattice Dynamics of hcp He^3 and He^4 at High Pressures*

G. L. Morley† and K. L. Kliewer

Institute for Atomic Research and Department of Physics, Iowa State University, Ames, Iowa 50010
(Received 15 July 1968; revised manuscript received 2 January 1969)

Calculations of the vibrational properties of hcp solid He^3 and He^4 at 0°K have been carried out. The harmonic coupling parameters for first and second neighbors have been evaluated for four molar volumes in the range 10.0 cm^3 to 16.0 cm^3 using the harmonic ground-state wave function and the self-consistent method of Koehler. The dispersion relations and sound velocities were evaluated for the symmetry directions Σ, T, and Δ. Frequency distribution functions and Debye temperatures at 0°K have also been obtained for both solids in the hcp phase. A comparison with experiment indicates that the calculated Debye temperatures are too high, the agreement with experiment being best at the highest density examined. The ratio of the He^3 Debye temperature to the He^4 Debye temperature Θ_3/Θ_4 at 0°K is found to be approximately 1.23 as compared with the classical value of 1.154 and the experimental value of 1.18.

I. INTRODUCTION

A theoretical study of the lattice dynamics of solid helium is complicated by the presence of a relatively large zero-point energy, a consequence of the small atomic mass and the weak forces between atoms. As a result of the large quantum effects, classical lattice dynamics fails as a method for determining the various vibrational properties of the solid. Classical lattice dynamics[1] gives imaginary frequencies for molar volumes of the solid larger than 12.6 cm^3.

In recent years several quantum-mechanical treatments have been presented for the determination of the ground-state energy of the solid.[2–8] Nosanow and co-workers,[9–14] in a series of papers, have calculated dispersion curves, Debye temperatures, etc., for the low-density bcc phase of He^3 and for low densities of hcp He^4. Nosanow *et al.* have used a variational method and a trial wave function composed of a product of single-particle functions centered about the lattice sites and short-range two-particle correlation functions.

Koehler[15–18] has developed a method of self-consistent lattice dynamics using a variational method with a ground-state harmonic wave function as a trial wave function. With the addition of short-range two-particle correlations to the trial wave function, Koehler[19] has calculated dispersion curves and the ground-state energy for bcc He^3.

The purpose of this work is to examine the vibrational properties of solid helium in the region of high densities. Previous theoretical results have been presented for molar volumes in the range 17.5 to 24.5 cm^3. The results presented here are for molar volumes in the region 10.0 to 16.0 cm^3 and for $T = 0°K$, conditions under which both He^3 and He^4 are in the hcp phase.

The self-consistent method of Koehler[15–18] modified for hcp symmetry is used in this calculation. The choice of trial wave function is that appropriate to a harmonic solid in the ground state. This particular choice of wave function suggests itself in the high-density case for several reasons. As the density of the solid increases, the effective single-particle potential shifts from one where the mean atomic position occurs at a relative potential maximum to one where the mean atomic position occurs at a potential minimum. Thus, the single-particle potential in the vicinity of the mean atomic position changes from a markedly anharmonic potential at low densities to a potential approximately harmonic at high densities. Accompanying this pronounced change in the potential shape is a relative decrease in the importance of the vibrational energy. At the lowest densities of the solid, the vibrational energy is of the same order of magnitude as the static lattice energy. As the density of the solid increases, however, the static lattice energy increases much faster than the vibrational energy. This means that as the density increases, the rms atomic displacements decrease more rapidly than the mean nearest-neighbor separation, thus tending to establish conditions for which the harmonic approximation is valid.

In addition, as the density increases long-range order should become the predominant effect. The harmonic ground-state wave function contains this long-range order implicitly. As a further point of interest, the results of Nosanow[11] indicate that the short-range correlations soften the repulsive core of the potential too much as the density of the solid is increased. This results in a lower bound on the range of densities considered. Thus less short-range correlation is needed as the density

increases, a conclusion which further commends the wave function used below.

II. GENERAL THEORY

Classical Lattice Dynamics

Consider a perfect crystal of solid helium in any of the three phases bcc, fcc, or hcp. Using periodic boundary conditions the Hamiltonian for any macrocell in the crystal is

$$H=\frac{1}{2M}\sum_{m\mu i}(p_{\mu i}^{m})^2 + \frac{1}{2}\sum_{\substack{m\mu\\ n\nu}}{}' v(|\vec{R}_\mu^{m}+\vec{q}_\mu^{m}-\vec{R}_\nu^{n}-\vec{q}_\nu^{n}|), \quad (2.1)$$

where M represents the mass of a helium atom and the prime on the second summation excludes those terms where $(m,\mu)=(n,\nu)$. The mean position and the displacement from the mean position of the μth atom in the mth cell are given by $\vec{R}_\mu^{m}$ and $\vec{q}_\mu^{m}$, respectively. The corresponding momentum in the Cartesian direction i is given by $p_{\mu i}^{m}$. The two particle interaction $v(r)$ is taken to be the Lennard-Jones potential

$$v(r)=4\epsilon[(\sigma/r)^{12}-(\sigma/r)^{6}]. \quad (2.2)$$

In the harmonic approximation (2.1) becomes

$$H_0=\frac{1}{2M}\sum_{m\mu i}(p_{\mu i}^{m})^2+\frac{1}{2}\sum_{\substack{m\mu\\ n\nu}}{}' v(|\vec{R}_\mu^{m}-\vec{R}_\nu^{n}|) + \frac{1}{2}\sum_{\substack{m\mu i\\ n\nu j}}\Phi_{\mu i,\nu j}^{mn}q_{\mu i}^{m}q_{\nu j}^{n}, \quad (2.3)$$

where the $\Phi_{\mu i,\nu j}^{mn}$ are the coupling parameters[20] of second order. In terms of normal coordinates (2.3) is

$$H_0=\frac{1}{2}\sum_{\vec{k}\lambda}\{P_\lambda^{\vec{k}}P_\lambda^{*\vec{k}}+\omega_{\vec{k}\lambda}^{2}Q_\lambda^{\vec{k}}Q_\lambda^{*\vec{k}}\} + \frac{1}{2}\sum_{\substack{m\mu\\ n\nu}}{}' v(|\vec{R}_\mu^{m}-\vec{R}_\nu^{n}|), \quad (2.4)$$

where the transformation

$$q_{\mu i}^{m}=\frac{1}{(NM)^{1/2}}\sum_{\vec{k}\lambda}e_{\mu i}(\vec{k},\lambda)Q_\lambda^{\vec{k}}\exp(i\vec{k}\cdot\vec{R}_\mu^{m}) \quad (2.5)$$

has been used.

The frequencies $\omega_{\vec{k}\lambda}$ and eigenvectors $e_{\mu i}(\vec{k},\lambda)$ are obtained from the set of equations

$$\sum_{\nu j}D_{ij}^{\mu\nu}(\vec{k})e_{j\nu}(\vec{k},\lambda)=\omega_{\vec{k}\lambda}^{2}e_{\mu i}(\vec{k},\lambda), \quad (2.6)$$

where $D_{ij}^{\mu\nu}(\vec{k})$ is the dynamical matrix defined by

$$D_{ij}^{\mu\nu}(\vec{k})=\frac{1}{M}\sum_{l}\Phi_{\mu i,\nu j}^{0l}\exp[i\vec{k}\cdot(\vec{R}_\nu^{l}-\vec{R}_\mu^{0})]. \quad (2.7)$$

For each $\vec{k}$, there are $3r$ modes of vibration $\omega_{\vec{k}\lambda}$, where r is the number of atoms in the unit cell. The quantity λ then indexes the different modes of vibration.

The exact ground-state wave function of the Hamiltonian given in (2.4) is

$$\Psi_0=A\exp[-\sum_{\vec{k}\lambda}(\omega_{\vec{k}\lambda}/2\hbar)Q_\lambda^{\vec{k}}Q_\lambda^{*\vec{k}}]. \quad (2.8)$$

Using the inverse transformation from normal to real coordinates (2.8) becomes

$$\Psi_0=A\exp\left(-\frac{1}{2}\sum_{\substack{m\mu i\\ n\nu j}}q_{\mu i}^{m}G_{\mu i,\nu j}^{mn}q_{\nu j}^{n}\right), \quad (2.9)$$

where

$$G_{\mu i\nu j}^{mn}=(M/\hbar N)\sum_{\vec{k}\lambda}\omega_{\vec{k}\lambda}e_{\mu i}^{*}(\vec{k},\lambda) \times e_{\nu j}(\vec{k},\lambda)\exp[i\vec{k}\cdot(\vec{R}_\nu^{n}-\vec{R}_\mu^{m})]. \quad (2.10)$$

The Ground-State Energy

Using the method of Koehler[17] we now evaluate the ground-state energy for the general Hamiltonian given in (2.1). In the variational calculation that follows, the wave function Ψ_0 (2.9) is used as a trial wave function for the general Hamiltonian with the frequencies $\omega_{\vec{k}\lambda}$ treated as variational parameters. The ground-state energy is

$$E_0=(1/2M)\sum_{m\mu i}(\Psi_0,(p_{\mu i}^{m})^2\Psi_0)/(\Psi_0,\Psi_0) + \frac{1}{2}\sum_{\substack{m\mu\\ n\nu}}{}'(\Psi_0,v(|\vec{x}_\mu^{m}-\vec{x}_\nu^{n}|)\Psi_0)/(\Psi_0,\Psi_0), \quad (2.11)$$

where $\vec{x}_\mu^{m}=\vec{R}_\mu^{m}+\vec{q}_\mu^{m}$. (2.12)

The kinetic energy term is the same as that present in the harmonic case so

$$\mathrm{KE} = (\hbar/4)\sum_{\vec{k}\lambda} \omega_{\vec{k}\lambda}. \tag{2.13}$$

The method of evaluation for the integrals in the potential energy term is similar to that given by Koehler.[17] The result of this evaluation is

$$\mathrm{PE} = \frac{1}{2} \sum_{\substack{m\mu \\ n\nu}}{}' \int v(|\vec{R}_{\mu\nu}^{\,mn} + \vec{q}|) P_{\mu\nu}^{\,mn}(\vec{q})\, d\vec{q}, \tag{2.14}$$

where

$$P_{\mu\nu}^{\,mn}(\vec{q}) = |(F_{\mu\nu}^{\,mn})^{-1}|^{1/2} \pi^{-3/2} \times \exp[-\tilde{q}(F_{\mu\nu}^{\,mn})^{-1} q], \tag{2.15}$$

and the abbreviations $\vec{R}_{\mu\nu}^{\,mn} = \vec{R}_{\mu}^{\,m} - \vec{R}_{\nu}^{\,n}$ and $\vec{q} = \vec{q}_{\mu}^{\,m} - \vec{q}_{\nu}^{\,n}$ have been used. q and $\tilde{q}$ are column and row representations of the vector $\vec{q}$. The function $P_{\mu\nu}^{\,mn}(\vec{q})$ represents a two-particle probability function for the relative displacement of the atoms (m, μ) and (n, ν) with the symmetry of the lattice appearing in the 3×3 matrix $F_{\mu\nu}^{\,mn}$ for each pair of atoms. The elements of this matrix are closely related to the $G_{\mu i,\nu j}^{\,mn}$ of (2.10) and are defined by

$$F_{\mu i,\nu j}^{\,mn} = (2\hbar/NM) \sum_{\vec{k}\lambda}{}' \omega_{\vec{k}\lambda}^{-1} e_{\mu i}^{*}(\vec{k},\lambda) \times \{e_{\mu j}(\vec{k},\lambda) - e_{\nu j}(\vec{k},\lambda) \times \exp[i\vec{k}\cdot(\vec{R}_{\nu}^{\,n} - \vec{R}_{\mu}^{\,m})]\}, \tag{2.16}$$

with the prime on the summation indicating that the $\vec{k} = 0$ acoustic modes are excluded.

The ground-state energy for the system is then

$$E_0 = (\hbar/4) \sum_{\vec{k}\lambda} \omega_{\vec{k}\lambda} + \frac{1}{2} \sum_{\substack{m\mu \\ n\nu}}{}' \int v(|\vec{R}_{\mu\nu}^{\,mn} + \vec{q}|) P_{\mu\nu}^{\,mn}(\vec{q})\, d\vec{q}. \tag{2.17}$$

The Minimization Conditions

We now require that the ground-state energy be a minimum with respect to the parameters $\omega_{\vec{k}\lambda}$. The $\omega_{\vec{k}\lambda}$ occur in $P_{\mu\nu}^{\,mn}(\vec{q})$ through the dependence of the matrix $F_{\mu\nu}^{\,mn}$ on the $\omega_{\vec{k}\lambda}$. Hence,

$$\frac{\partial E_0}{\partial \omega_{\vec{k}\lambda}} = \frac{\hbar}{4} + \frac{1}{2} \sum_{\substack{m\mu \\ n\nu}}{}' \int v(|\vec{R}_{\mu\nu}^{\,mn} + \vec{q}|) \times \frac{\partial P_{\mu\nu}^{\,mn}(\vec{q})}{\partial \omega_{\vec{k}\lambda}}\, d\vec{q}. \tag{2.18}$$

Differentiating $P_{\mu\nu}^{\,mn}(\vec{q})$ with respect to $\omega_{\vec{k}\lambda}$ and integrating by parts then yields

$$\frac{\partial E_0}{\partial \omega_{\vec{k}\lambda}} = \frac{\hbar}{4} + \frac{1}{8} \sum_{\substack{m\mu i \\ n\nu j}}{}' \frac{\partial F_{\mu i,\nu j}^{\,mn}}{\partial \omega_{\vec{k}\lambda}} \times \int \frac{\partial^2 v(|\vec{R}_{\mu\nu}^{\,mn} + \vec{q}|)}{\partial q_i \partial q_j} P_{\mu\nu}^{\,mn}(\vec{q})\, d\vec{q}. \tag{2.19}$$

The remaining integral represents the expectation value of $\partial^2 v/\partial q_i \partial q_j$ with respect to the weight function $P_{\mu\nu}^{\,mn}$. This expectation value replaces the second-order coupling parameters which appear in classical lattice dynamics. By analogy we define

$$\Phi_{\mu i,\,\nu j}^{\,mn} = -\int \frac{\partial^2 v(|\vec{R}_{\mu\nu}^{\,mn} + \vec{q}|)}{\partial q_i \partial q_j} P_{\mu\nu}^{\,mn}(\vec{q})\, d\vec{q}, \tag{2.20a}$$

where $(m, \mu) \neq (n, \nu)$, and

$$\Phi_{\mu i,\,\nu j}^{\,mm} = -\sum_{n\nu}{}' \Phi_{\mu i,\nu j}^{\,mn} \tag{2.20b}$$

The minimization condition is then

$$\frac{\partial E_0}{\partial \omega_{\vec{k}\lambda}} = \frac{\hbar}{4} - \frac{1}{8} \sum_{\substack{m\mu i \\ n\nu j}}{}' \Phi_{\mu i \nu j}^{\,mn} \frac{\partial F_{\mu i,\nu j}^{\,mn}}{\partial \omega_{\vec{k}\lambda}} = 0 \tag{2.21}$$

Introducing the derivative of $F_{\mu i,\nu j}^{\,mn}$ with respect to $\omega_{\vec{k}\lambda}$ and rearranging terms, we obtain for the minimization condition

$$\frac{1}{NM} \sum_{\substack{m \\ n\nu j}} \Phi_{\mu i,\,\nu j}^{\,mn} \exp[i\vec{k}\cdot(\vec{R}_{\nu}^{\,n} - \vec{R}_{\mu}^{\,m})] \times e_{\nu j}(\vec{k},\lambda) = \omega_{\vec{k}\lambda}^{2} e_{\mu i}(\vec{k},\lambda), \tag{2.22}$$

which is equivalent to (2.6).

This final form for the minimization condition (2.22) corresponds to the eigenvalue problem of classical lattice dynamics. There are, however, some significant differences: (1) the coupling parameters $\Phi_{\mu i,\,\nu j}^{\,mn}$ depend on the frequencies $\omega_{\vec{k}\lambda}$ so the set of equations (2.15), (2.16), (2.20), and (2.22) must be solved self-consistently; (2) the coupling parameters contain anharmonic effects, which can be simply demonstrated by expanding $\partial^2 v/\partial q_i \partial q_j$ for small q; and (3) the coupling parameters are determined by a quantum-mechanical average.

III. HEXAGONAL CLOSE-PACKED STRUCTURE

In this section the general theory is applied to the specific case of a hexagonal close-packed lattice. The positions of the lattice sites surrounding the origin are labeled by

$$\vec{R}^{p} = \vec{R}_{\nu}{}^{l} - \vec{R}_{1} = \vec{R}^{l} + \vec{R}_{\nu} , \tag{3.1}$$

where

$$\vec{R}^{l} = (l_1 - \tfrac{1}{2} l_2) a\hat{i}_1 + (\sqrt{3}/2) l_2 a\hat{i}_2 + l_3 c\hat{i}_3 , \tag{3.2}$$

with $\hat{i}_1$, $\hat{i}_2$, and $\hat{i}_3$ being unit vectors in the x, y, and z directions, respectively, and x is directed along the nearest-neighbor line in the basal plane. The quantity a represents the cell constant in the basal plane and c represents the cell constant in the z direction. The unit cell integers l_1, l_2, l_3 and the components of $\vec{R}^{l}$ are listed in Table I for the first 12 neighbors of the lattice site at the origin.

TABLE I. Positions of the first 12 lattice sites.

p	ν	l_1	l_2	l_3	$R_x{}^{p}$	$R_y{}^{p}$	$R_z{}^{p}$
0	1	0	0	0	0	0	0
1	1	1	0	0	a	0	0
2	1	1	1	0	$a/2$	$3^{1/2}a/2$	0
3	1	0	1	0	$-a/2$	$3^{1/2}a/2$	0
4	1	−1	0	0	$-a$	0	0
5	1	−1	−1	0	$-a/2$	$-3^{1/2}a/2$	0
6	1	0	−1	0	$a/2$	$-3^{1/2}a/2$	0
7	2	−1	−1	−1	0	$-a/3^{1/2}$	$-c/2$
8	2	−1	−1	0	0	$-a/3^{1/2}$	$c/2$
9	2	−1	0	−1	$-a/2$	$a/2\times 3^{1/2}$	$-c/2$
10	2	−1	0	0	$-a/2$	$a/2\times 3^{1/2}$	$c/2$
11	2	0	0	−1	$a/2$	$a/2\times 3^{1/2}$	$-c/2$
12	2	0	0	0	$a/2$	$a/2\times 3^{1/2}$	$c/2$

The wave vector, $\vec{k}$ in this case is

$$\vec{k} = \frac{2\pi}{L}\left(\frac{n_1\hat{i}_1}{a} + \frac{(n_1+2n_2)\hat{i}_2}{\sqrt{3}a} + \frac{n_3\hat{i}_3}{c}\right) , \tag{3.3}$$

This vector $\vec{k}$ is restricted to the first Brillouin zone by requiring that

$$|2n_1 + n_2| \leq L , \tag{3.4a}$$

and

$$|2n_3| \leq L , \tag{3.4b}$$

where $L^3 = N$, the number of unit cells. The first Brillouin zone is shown in Fig. 1.

The method of Begbie and Born[21] is used to reduce the number of coupling parameters that need be considered. A summary of the coupling parameters between the first 12 neighbors and the atom at the origin is found in Table II.

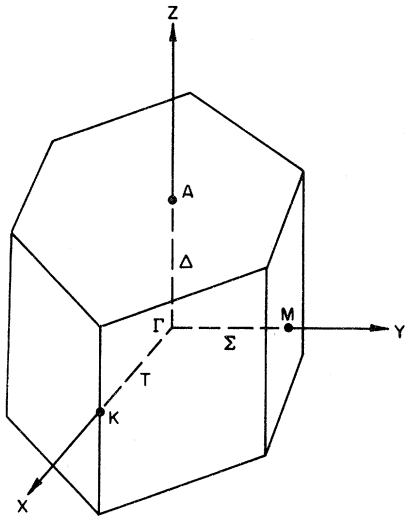

FIG. 1. First Brillouin zone for the hcp lattice.

TABLE II. Coupling parameters for the first 12 neighbors.

p	$-\Phi_{11}{}^{p}$	$-\Phi_{22}{}^{p}$	$-\Phi_{33}{}^{p}$	$-\Phi_{12}{}^{p}$	$-\Phi_{23}{}^{p}$	$-\Phi_{13}{}^{p}$
0	$-6(\alpha+\lambda)$	$-6(\alpha+\lambda)$	$-6(\gamma+\nu)$	0	0	0
1	$\alpha+2\beta$	$\alpha-2\beta$	γ	0	0	0
2	$\alpha-\beta$	$\alpha+\beta$	γ	$3^{1/2}\beta$	0	0
3	$\alpha-\beta$	$\alpha+\beta$	γ	$-3^{1/2}\beta$	0	0
4	$\alpha+2\beta$	$\alpha-2\beta$	γ	0	0	0
5	$\alpha-\beta$	$\alpha+\beta$	γ	$3^{1/2}\beta$	0	0
6	$\alpha-\beta$	$\alpha+\beta$	γ	$-3^{1/2}\beta$	0	0
7	$\lambda+2\mu$	$\lambda-2\mu$	ν	0	-2σ	0
8	$\lambda+2\mu$	$\lambda-2\mu$	ν	0	2σ	0
9	$\lambda-\mu$	$\lambda+\mu$	ν	$3^{1/2}\mu$	σ	$-3^{1/2}\sigma$
10	$\lambda-\mu$	$\lambda+\mu$	ν	$3^{1/2}\mu$	$-\sigma$	$3^{1/2}\sigma$
11	$\lambda-\mu$	$\lambda+\mu$	ν	$-3^{1/2}\mu$	σ	$3^{1/2}\sigma$
12	$\lambda-\mu$	$\lambda+\mu$	ν	$-3^{1/2}\mu$	$-\sigma$	$-3^{1/2}\sigma$

It should be noted that to insure that the anisotropic stresses within the crystal vanish at equilibrium, it is necessary to place an additional restriction on the coupling parameters, [22] a consequence of rotational invariance within the crystal. When the external stresses either vanish or are a result of hydrostatic pressure, the condition is

$$3c^2\lambda/2a^2 = 3\gamma + \nu \ . \tag{3.5}$$

The Dynamical Matrix

The dynamical matrix can be written in the form

$$D(\vec{k}) = \begin{pmatrix} A(\vec{k}) & B(\vec{k}) \\ B^*(\vec{k}) & A(\vec{k}) \end{pmatrix}, \tag{3.6}$$

where $A(\vec{k})$ and $B(\vec{k})$ are 3×3 matrices defined by

$$A(\vec{k}) = \sum_{p=0}^{6} (\Phi^p/M)\exp(i\vec{k}\cdot\vec{R}^p), \tag{3.7a}$$

and $$B(\vec{k}) = \sum_{p=7}^{12} (\Phi^p/M)\exp\{i\vec{k}\cdot\vec{R}^p\} \ , \tag{3.7b}$$

with Φ^p defined by Table II. The elements of $A(\vec{k})$ and $B(\vec{k})$ are given in Appendix A.

The matrix $D(\vec{k})$ and the eigenvectors $e(\vec{k},\lambda)$, are complex quantities. In order to solve for the frequencies numerically, it is convenient to transform these quantities into a system where they are real. The matrix $B(\vec{k})$ can be written

$$B(\vec{k}) = B'(\vec{k}) + iB''(\vec{k}) \ , \tag{3.8}$$

where $B'(\vec{k})$ and $B''(\vec{k})$ are both real. Using the unitary transformation,

$$T = \frac{1}{\sqrt{2}}\begin{pmatrix} I & I \\ -iI & iI \end{pmatrix}, \tag{3.9}$$

the eigenvalue problem becomes one of solving the set of equations

$$\mathfrak{D}(\vec{k})E(\vec{k},\lambda) = \omega_{\vec{k}\lambda}{}^2 E(\vec{k},\lambda) \ , \tag{3.10}$$

where

$$\mathfrak{D}(\vec{k}) = TD(\vec{k})T^{-1} = \begin{pmatrix} A+B' & B'' \\ B'' & A-B' \end{pmatrix}, \tag{3.11}$$

and $$E(\vec{k},\lambda) = Te(\vec{k},\lambda) \ . \tag{3.12}$$

The new matrix $\mathfrak{D}(\vec{k})$ is both real and symmetric.

The Matrix $F_{\mu\nu}{}^{mn}$

The next problem is to express the matrix $F_{\mu\nu}{}^{mn}$ for the hcp structure in a usable form. Using the notation $F^p = F_{1\nu}{}^{0l}$, Eq. (2.16) can be expressed as

$$F_{ij}{}^p = (2\hbar/NM)\sum_n \sum_\lambda \omega_{n\lambda}{}^{-1} \sum_{\{n\}} e_{1i}{}^*(\{n\};\lambda)$$
$$\times\Big\{e_{1j}(\{n\};\lambda) - e_{\nu j}(\{n\};\lambda)$$
$$\times\exp\Big[i\frac{2\pi}{L}\Big(\frac{n_1}{a}R_x{}^p + \frac{n_1+2n_2}{3^{1/2}}R_y{}^p + \frac{n_3}{c}R_z{}^p\Big)\Big]\Big\} \tag{3.13}$$

where n refers to a point in the irreducible part of the Brillouin zone, and $\{n\}$ designates a point outside of the irreducible part of the zone but equivalent to n. Because of the symmetry of the lattice, Eq. (3.13) need only be evaluated for $p=1$ and 8. This is sufficient to determine the matrices Φ^1 and Φ^8 which contain all of the coupling parameter components. The elements of F^1 and F^8 are given in Appendix B.

The Coupling Parameter Integrals

In the hcp case the probability function (2.15) for the pairs of atoms $p=1$ and 8 becomes

$$P^1(\vec{x}-\vec{R}^1) = C_1\exp[-(x_1-a)^2/F_{11}{}^1 - x_2{}^2/F_{22}{}^1 - x_3{}^2/F_{33}{}^1] \ , \tag{3.14a}$$

and

$$P^8(\vec{x}-\vec{R}^8) = C_8\exp\{-x_1{}^2/F_{11}{}^8 - [F_{22}{}^8F_{33}{}^8 - (F_{23}{}^8)^2]^{-1} \times[F_{33}{}^8(x_2+a/\sqrt{3})^2 - 2F_{23}{}^8(x_2+a/\sqrt{3})(x_3-c/2) + F_{22}{}^8(x_3-c/2)^2]\} \ , \tag{3.14b}$$

where x_1, x_2, and x_3 are Cartesian components of the vector $\vec{x} = \vec{q} + \vec{R}^p$. The coefficients C_1 and C_8 are defined by

$$C_1 = 1/(\pi^{3/2}|F^1|^{1/2}) \ , \tag{3.15a}$$

and $$C_8 = 1/(\pi^{3/2}|F^8|^{1/2}) \ . \tag{3.15b}$$

The coupling parameters given in Table II can now be determined from (2.20):

$$\Phi_{ij}{}^p = -\int\{x_ix_jf(x) + \delta_{ij}g(x)\}P^p(\vec{x}-\vec{R}^p)d\vec{x} \ , \tag{3.16}$$

where $$f(x) = -v'(x)/x^3 + v''(x)/x \tag{3.17}$$

and $$g(x) = v'(x)/x \ . \tag{3.18}$$

$v'(x)$ and $v''(x)$ are the first and second deriva-

tives of the potential function $v(x)$.

The expressions for α, β, γ, λ, μ, ν, and σ are found in Appendix C.

This completes the determination of the set of equations necessary for evaluating the coupling parameters self-consistently for the hcp lattice. The following procedure is used in the actual calculation. An initial set of coupling parameters is assumed. These parameters are used to evaluate the dynamical matrix $\mathfrak{D}(\vec{k})$. This matrix is then diagonalized to find the frequencies $\omega_{\vec{k}\lambda}$ and eigenvectors $E(\vec{k},\lambda)$. The frequencies and eigenvectors are then used to evaluate the matrices F^{p} which in turn determine the probability functions $P^{p}(\vec{q})$. To complete the cycle, the coupling parameters are found by evaluating the integrals (3.16) numerically. The process is repeated until the coupling parameters in succesive iterations differ by no more than one part in 10^3.

IV. RESULTS

The Coupling Parameters

The set of self-consistent equations described in the preceding section has been solved numerically on the Iowa State University IBM 360-50 computer, using as parameters in the Lennard-Jones potential (2.2) $\epsilon = 14.1\times10^{-16}$ ergs and $\sigma = 2.56$ Å. One complete cycle of the iteration requires approximately 3 min. The integrals given in Eq. (C1) of Appendix C are expressed in terms of spherical coordinates and then integrated numerically. The lower limit of integration on the radial integral was set at 1 Å. This choice is somewhat arbitrary for molar volumes less than 13.0 cm^3, as the lower limit of integration can be varied throughout a region about 1 Å without affecting the values of the integrals. In Fig. 2 a plot of the integrand $I_\nu(\rho)$ of the radial integral of Eq. (C1f) is given as an illustration. For larger molar volumes the value of the integral becomes increasingly dependent on the choice of the lower limit of integration as is clear from Fig. 2. This difficulty is due to the lack of sufficient short-range correlation in the wave function for the larger molar volumes, and indicates explicitly that the present theory is indeed a high-density theory.

In the numerical calculations the ideal hcp ratio, $c/a=\sqrt{8/3}$, has been assumed. In this case the first 12 lattice sites given in Table I are all nearest-neighbor lattice sites. The self-consistent coupling parameters retaining only nearest-neighbor interactions are given in Tables III and IV for four molar volumes.

The case where the first 18 neighbors are included has also been examined for the molar volume range 10 to 16 cm^3. The change in nearest-neighbor parameters α, β, γ, λ, μ, ν, and σ is

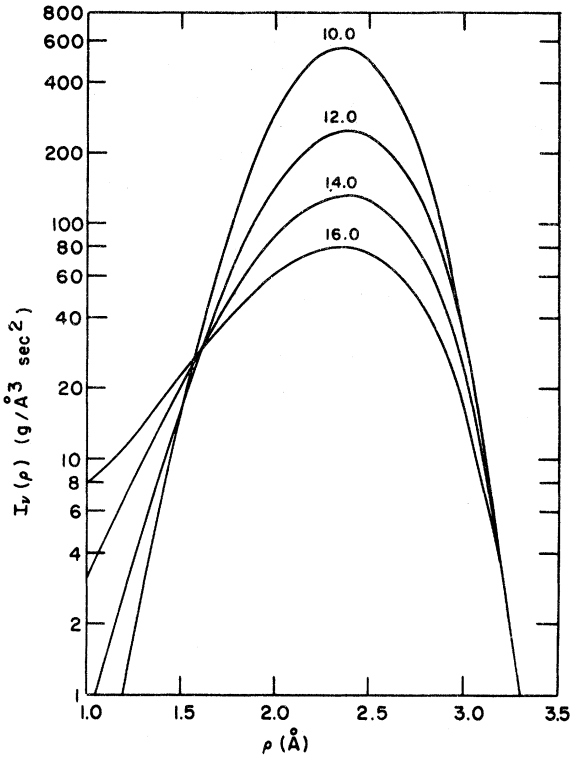

FIG. 2. The radial integrand $I_\nu(\rho)$ of Eq. (C1f) as a function of ρ for four molar volumes.

TABLE III. He^3 nearest-neighbor coupling parameters (in dyn/cm).

	V_m(cm^3)			
	10.0	12.0	14.0	16.0
α	1720	700	339	192
β	920	360	166	90.5
γ	6.8	8.5	6.4	6.1
λ	97.8	57.6	36.8	26.0
μ	−63.4	−36.3	−21.7	−14.8
ν	372	205	128	88.7
σ	−158	−87.7	−54.0	−36.9

TABLE IV. He^4 nearest-neighbor coupling parameters (in dyn/cm).

	V_m(cm^3)			
	10.0	12.0	14.0	16.0
α	1660	640	302	165
β	885	325	145	75.1
γ	3.0	5.4	5.8	5.1
λ	84.6	47.9	31.1	21.8
μ	−55.0	−29.2	−18.7	−12.1
ν	330	174	107	73.0
σ	−139	−73.3	−44.9	−30.2

less than 0.3%. The second-neighbor parameters are small, of the order of 1 or 2 dyn/cm. The fact that the second-neighbor parameters are small can be understood in the following way. We have made a calculation of the first- and second-neighbor coupling parameters in the classical quasiharmonic approximation. The result is that the average second-neighbor coupling parameter is approximately 0.9% of the average nearest-neighbor coupling parameter for a molar volume of 10.0 cc, 1.2% for

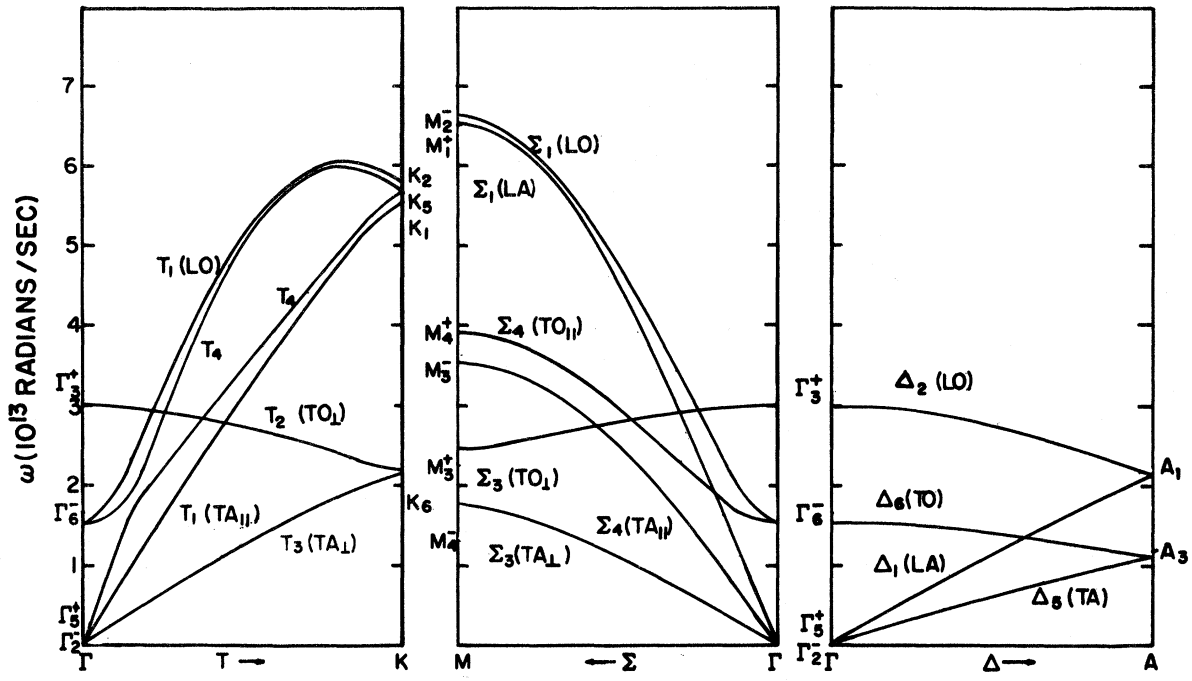

FIG. 3. He^3 dispersion curves for $V_m = 10.0$ cm^3.

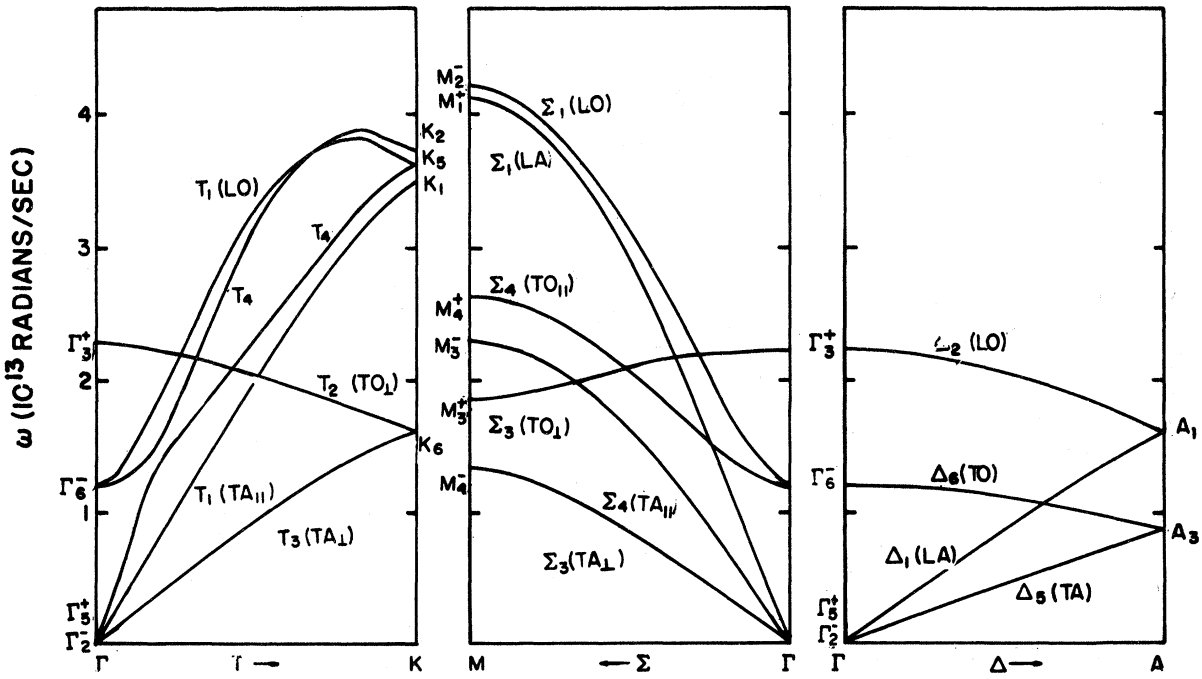

FIG. 4. He^3 dispersion curves for $V_m = 12.0$ cm^3.

a molar volume of 12.0 cc, and 12.3% for a molar volume of 14.0 cc. In the quantum-mechanical calculation the coupling parameters are increased in magnitude by contributions from the core of the potential. Since this effect is considerably larger for nearest neighbors than for second neighbors, the relative smallness of the second-neighbor parameters results.

The Dispersion Relations

Dispersion relations have been evaluated for three symmetry directions, Δ, Σ, and T of Fig. 1, using the nearest-neighbor coupling parameters of Tables III and IV. The dispersion relations for He^3 are given in Figs. 3–6. The dispersion relations for He^4 are very similar to those for He^3.

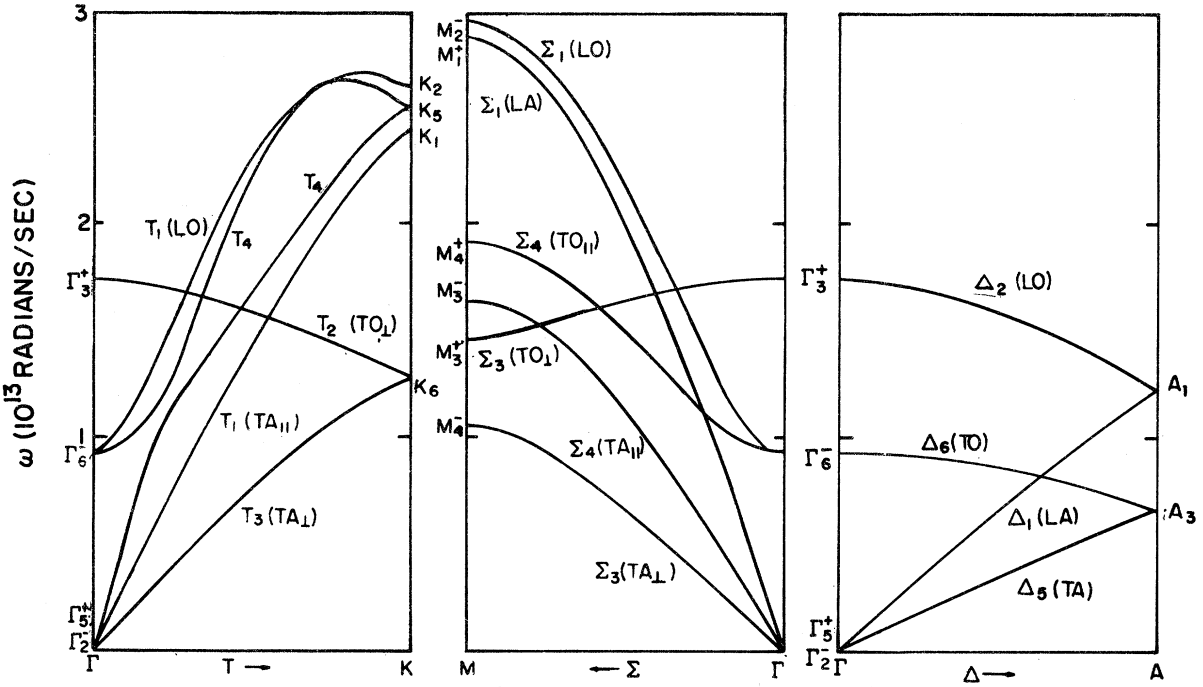

FIG. 5. He^3 dispersion curves for $V_m = 14.0$ cm^3.

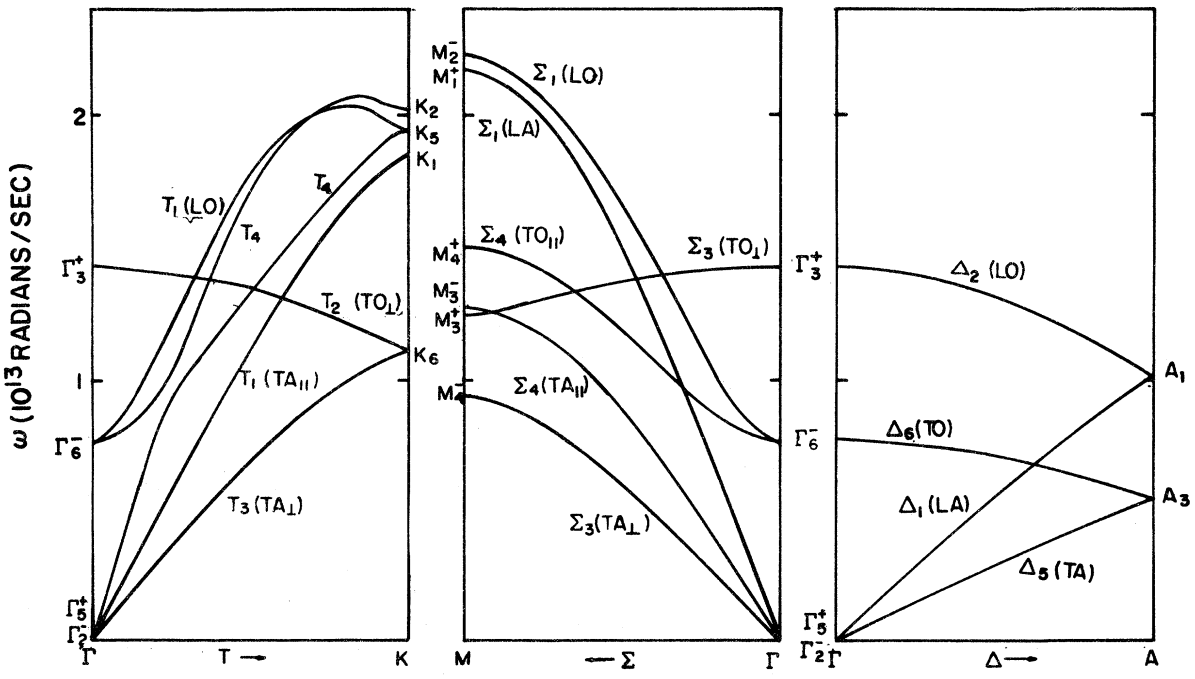

FIG. 6. He^3 dispersion curves for $V_m = 16.0$ cm^3.

Raubenheimer and Gilat[23] have listed the allowable irreducible representations for the high-symmetry directions and points of the hcp lattice, together with the corresponding compatibility relations. These compatibility relations together with the properties of the eigenvectors were used in labeling the dispersion curves in Figs. 3–6.

An interesting feature of these dispersion curves is that the transverse acoustic modes are widely separated in the Σ and T directions implying a high degree of anisotropy.

The Frequency Distribution Function

The numerical method of Raubenheimer and Gilat[23] has been used to evaluate the frequency distribution function, $G(\omega)$, at several molar volumes for both He^3 and He^4. The unnormalized $G(\omega)$ given in Figs. 7–10 were obtained using a mesh of 960 points in the irreducible part of the first Brillouin zone and 1000 channels for ω. The calculation for each $G(\omega)$ requires 9 min on the Iowa State University IBM 360-50 computer. The results for He^4 are again similar. A summary of the critical points in the symmetry directions Δ, Σ, and T is found in Tables V and VI. The symmetry directions Δ, Σ, and T account for most of the significant critical points in Figs. 7–10. However, there is at least one strong critical point not connected with these symmetry directions. This point lies between the critical points M_4^- and K_6. There may also be another strong critical point near T_4. The critical points Γ_6^-, K_1, K_2, and $T_1(\mathrm{LO})$ all appear to be quite weak or non-existent.

The Debye Temperature

The frequency distribution functions have been used to determine the Debye characteristic temperature at 0°K. In the Debye region the distribution function has the form

$$g(\omega) = c_0\omega^2 , \tag{4.1}$$

where c_0 is a constant determined by fitting in this case. The Debye characteristic temperature Θ can be calculated from the equation

$$\Theta = (\hbar/k)(3A_0/2c_0)^{1/3} , \tag{4.2}$$

where k is Boltzman's constant and A_0 is the total area under the complete distribution function curve. The results of this calculation are given in Table VII.

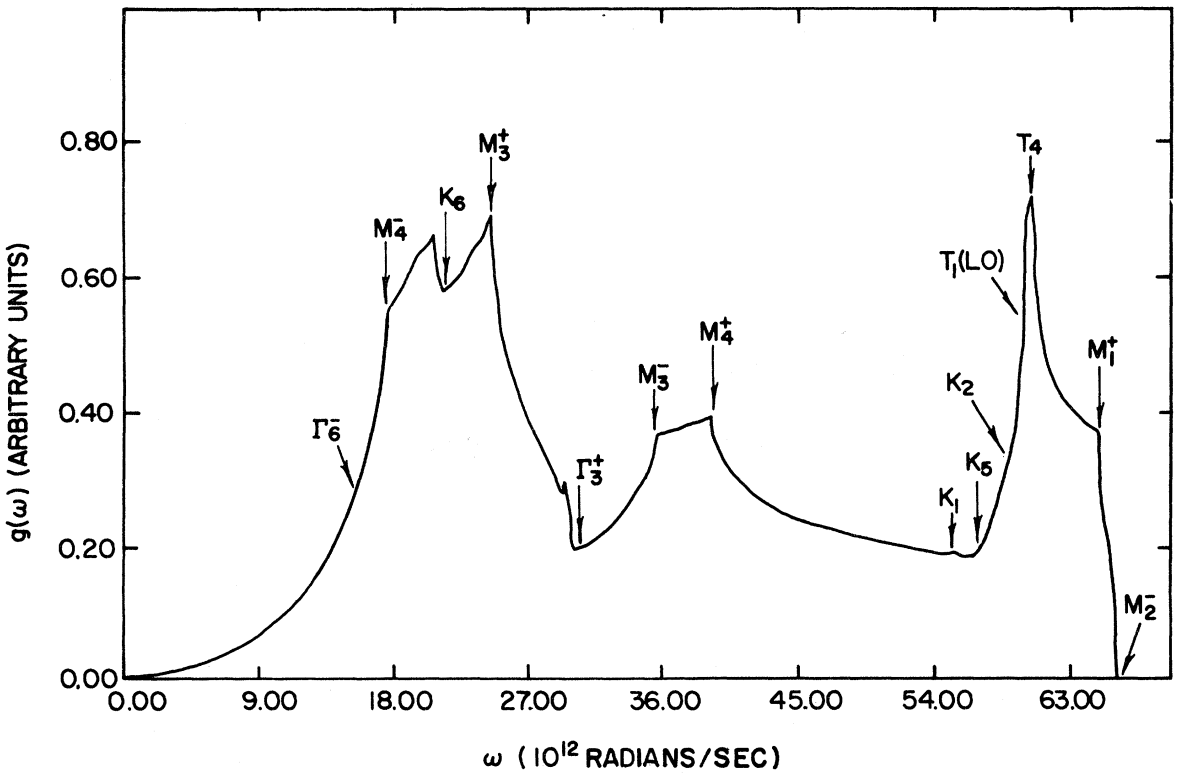

FIG. 7. He^3 frequency distribution for $V_m = 10.0$ cm^3.

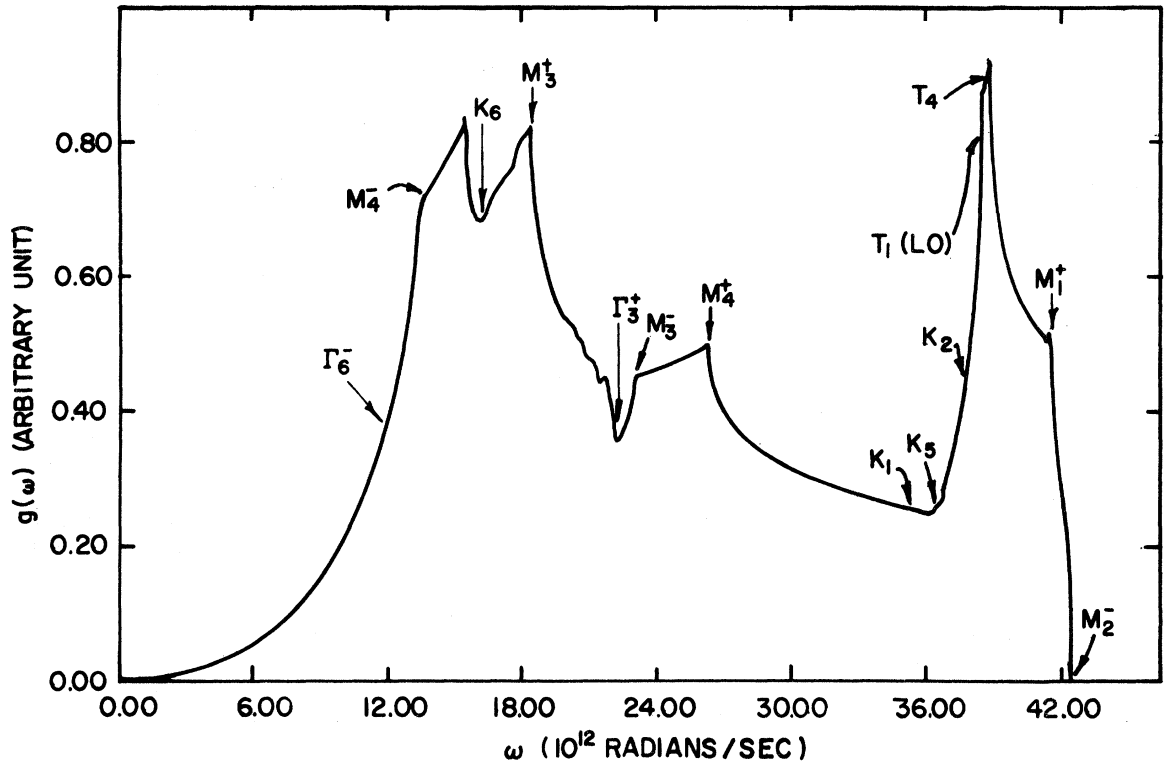

FIG. 8. He^3 frequency distribution for $V_m = 12.0$ cm^3.

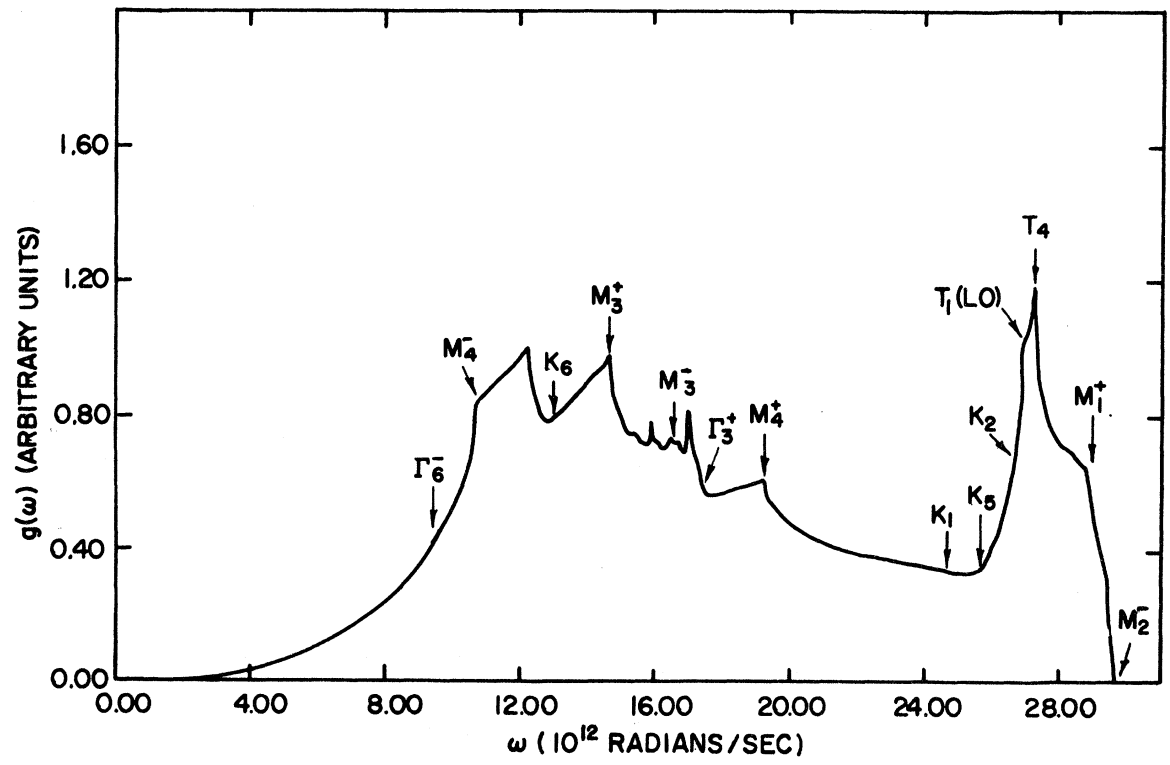

FIG. 9. He^3 frequency distribution for $V_m = 14.0$ cm^3

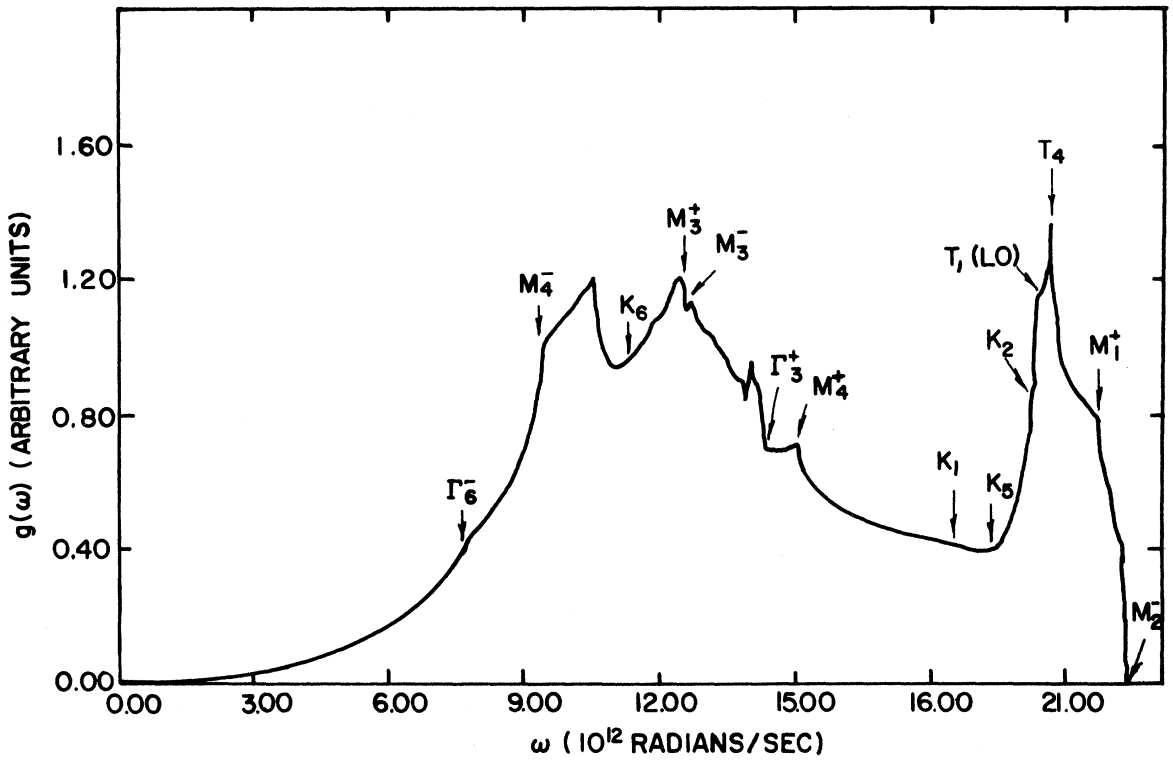

FIG. 10. He^3 frequency distribution for $V_m = 16.0$ cm^3.

TABLE V. Critical points for He^3 in Δ, Σ, and T directions.

Point	ω (10^{12} rad/sec) 10.0 cm^3/mole	12.0 cm^3/mole	14.0 cm^3/mole	16.0 cm^3/mole
Γ_6^-	15.3	11.7	9.39	7.89
Γ_3^+	29.8	22.2	17.5	14.6
M_4^-	17.5	13.3	10.6	8.98
M_3^+	24.6	18.5	14.7	12.3
M_3^-	35.4	23.0	16.5	12.6
M_4^+	39.2	26.3	19.2	15.1
M_1^+	65.4	41.7	28.8	21.7
M_2^-	66.3	42.4	29.5	22.3
K_6	21.4	16.2	12.8	10.8
K_1	55.3	35.2	24.5	18.5
K_5	56.6	36.4	25.6	19.4
K_2	58.0	37.6	26.6	20.3
$T_1(LO)_{\max}$	60.1	38.5	26.9	20.3
T_4 max	60.6	38.9	27.2	20.7

The classical value for the ratio of Debye temperatures Θ_3/Θ_4 is

$$\Theta_3/\Theta_4 = (M_4/M_3)^{1/2} = 1.154 , \qquad (4.3)$$

where M_3 and M_4 refer to the masses of the He^3 and He^4 atoms, respectively. Sample and Swenson's[24] measurements give $\Theta_3/\Theta_4 = 1.18$. Calculated Debye temperatures Θ_3 and Θ_4 are plotted in Fig. 11 as a function of molar volume. The results of Nosanow and Werthamer's[13] He^4 hcp calculation and the experimental data of Sample and Swenson,[24] Heltemes and Swenson,[25] and Franck[26] are also plotted.

TABLE VI. Critical points for He^4 in Δ, Σ, and T directions.

Point	ω (10^{12} rad/sec) 10.0 cm^3/mole	12.0 cm^3/mole	14.0 cm^3/mole	16.0 cm^3/mole
Γ_6^-	12.4	9.30	7.49	6.27
Γ_3^+	24.4	17.7	13.9	11.5
M_4^-	14.2	10.5	8.45	7.08
M_3^+	20.0	14.7	11.7	9.70
M_3^-	30.3	19.3	13.6	10.3
M_4^+	33.2	21.7	15.8	12.2
M_1^+	55.7	34.4	23.5	17.3
M_2^-	56.4	35.0	24.1	17.8
K_6	17.4	12.8	10.2	8.54
K_1	47.2	29.3	20.1	14.9
K_5	48.2	30.2	20.9	15.6
K_2	49.2	31.0	21.7	16.3
$T_1(LO)_{\max}$	51.2	31.9	22.0	16.3
$T_{4\ \max}$	51.5	32.1	22.2	16.6

TABLE VII. Debye temperatures for He^3 and He^4 at 0°K.

V_m(cm^3)	θ_3 (°K)	θ_4 (°K)	θ_3/θ_4
10.0	255	211	1.21
12.0	187	151	1.24
14.0	145	118	1.23
16.0	119	95	1.25

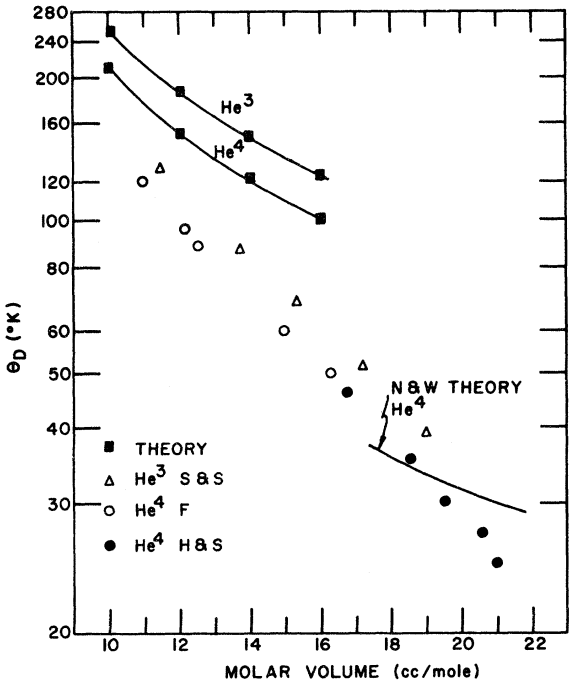

FIG. 11. Debye temperatures at 0°K.

The Sound Velocities

Calculated sound velocities for He^3 are given in Fig. 12 for several molar volumes. Similar results have been obtained for He^4. The sound velocities were determined by finding the change in $\omega_{\vec{k}\lambda}$ for changes in $\vec{k}$ at small k. The transverse and longitudinal sound velocities shown in Fig. 12 reflect the cylindrical symmetry appropriate in the

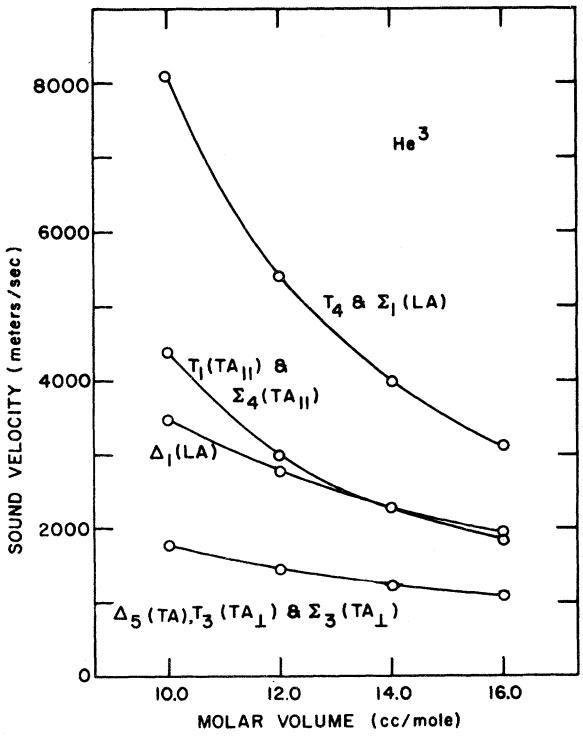

FIG. 12. He^3 velocities of sound at 0°K.

case where the crystal symmetry is hcp. An interesting aspect of the results is the large anisotropy of the sound velocities which, because of the symmetry, is a function only of the angular deviation from the basal plane. For example, the longitudinal sound velocity in the basal plane is larger than that of the Δ direction by a factor of 2 or 3.

The Elastic Constants

The elastic constants can be calculated from the coupling parameters given in Tables III and IV using the relations[21]

$$c_{11} = (2/3^{1/2}c)(-2\mu^2/\lambda + 3\alpha + 3\beta + \lambda - \mu), \quad (4.4a)$$

$$c_{12} = (2/3^{1/2}c)(2\mu^2/\lambda - 3\alpha + 9\beta - \lambda - 3\mu), \quad (4.4b)$$

$$c_{33} = 3^{1/2}c\nu/a^2, \quad (4.4c)$$

$$c_{44} = 3^{1/2}c\lambda/a^2, \quad (4.4d)$$

and

$$c_{13} = -(4\sigma/a + 3^{1/2}c\lambda/a^2), \quad (4.4e)$$

where c and a are the appropriate lattice parameters.

Discussion

The Debye characteristic temperatures at 0°K provide one of the few tests for comparison of the calculations with experin ental data. As was expected the agreement with experiment becomes worse as the molar volume increases. The theoretical values for $V_m = 14.0$ cm^3 and $V_m = 16.0$ cm^3 are much higher than the experimental results. On the other hand, the calculated Debye temperatures for $V_m = 12.0$ cm^3 and $V_m = 10.0$ cm^3 are much more reasonable. This agrees with the original conjecture that the theory should be more appropriate at the higher densities of the solid.

It is interesting to note that the calculated ratio $\Theta_3/\Theta_4 \cong 1.23$ is fairly consistent throughout the range of molar volumes indicating a significant departure of the Debye temperatures from the classical mass dependence.

The calculations presented here are for molar volumes ranging from 10.0 to 16.0 cm^3. Extending the calculation downward to 8.0 cm^3 yields no anomalous results.

APPENDIX A. THE MATRICES $A(\vec{k})$ AND $B(\vec{k})$

Evaluation of the elements of the matrices $A(\vec{k})$ and $B(\vec{k})$ using (3.3), (3.7), Table I, and Table II yields

$$A_{11} = (1/M)\{6\lambda + 2(\alpha + 2\beta)[1 - \cos2\Theta_1] + 2(\alpha - \beta)[2 - \cos2\Theta_2 - \cos2(\Theta_1 + \Theta_2)]\}, \quad (A1a)$$

$$A_{22} = (1/M)\{6\lambda + 2(\alpha - 2\beta)[1 - \cos2\Theta_1] + 2(\alpha + \beta)[2 - \cos2\Theta_2 - \cos2(\Theta_1 + \Theta_2)]\}, \quad (A1b)$$

$$A_{33} = (1/M)\{6\nu + 2\gamma[3 - \cos2\Theta_1 - \cos2\Theta_2 - \cos2(\Theta_1 + \Theta_2)]\}, \quad (A1c)$$

$$A_{12} = (2\sqrt{3}\beta/M)\{\cos2\Theta_2 - \cos2(\Theta_1 + \Theta_2)\}, \quad (A1d)$$

and $$A_{13} = A_{23} = 0, \quad (A1e)$$

where $\Theta_1 = \pi m_1/L$, and $\Theta_2 = \pi m_2/L$, and

$$B_{11} = -(2/M)[(\lambda + 2\mu)e^{-2i\varphi} + 2(\lambda - \mu)\cos\Theta_1 e^{i\varphi}]\cos\Theta_3, \quad (A2a)$$

$$B_{22} = -(2/M)[(\lambda - 2\mu)e^{-2i\varphi} + 2(\lambda + \mu)\cos\Theta_1 e^{i\varphi}]\cos\Theta_3, \quad (A2b)$$

$$B_{33} = -(2\nu/M)[e^{-2i\varphi} + 2\cos\Theta_1 e^{i\varphi}]\cos\Theta_3, \quad (A2c)$$

$$B_{12} = (4\sqrt{3}\mu i/M)\sin\Theta_1 e^{i\varphi}\cos\Theta_3, \quad (A2d)$$

$$B_{13} = -(4\sqrt{3}\sigma/M)\sin\Theta_1 e^{i\varphi}\sin\Theta_3, \quad (A2e)$$

and

$$B_{23} = -(4i\sigma/M)[e^{-2i\varphi} - \cos\Theta_1 e^{i\varphi}]\sin\Theta_3, \quad (A2f)$$

where $\Theta_3 = \pi m_3/L$ and $\varphi = \pi(n_1 + 2n_2)/3L$.

APPENDIX B. THE MATRIX F^p

Matrices F^1 and F^8 are symmetric with elements

$$F_{11}{}^1 = \sum_n (\hbar N_n/3NM)\sum_\lambda \omega_{n\lambda}{}^{-1}\{(E_1{}^2 + E_4{}^2)[\tfrac{3}{2} - \cos2\Theta_1 - \tfrac{1}{4}\cos2\Theta_2 - \tfrac{1}{4}\cos2(\Theta_1 + \Theta_2)] + \tfrac{3}{4}(E_2{}^2 + E_5{}^2)[2 - \cos2\Theta_2 - \cos2(\Theta_1 + \Theta_2)] + (\sqrt{3}/2)(E_1E_2 + E_4E_5)[\cos2\Theta_2 - \cos2(\Theta_1 + \Theta_2)]\}, \quad (B1a)$$

$$F_{22}{}^1 = \sum_n (\hbar N_n/3NM)\sum_\lambda \omega_{n\lambda}{}^{-1}\{(E_2{}^2 + E_5{}^2)[\tfrac{3}{2} - \cos2\Theta_1 - \tfrac{1}{4}\cos2\Theta_2 - \tfrac{1}{4}\cos2(\Theta_1 + \Theta_2)] + \tfrac{3}{4}(E_1{}^2 + E_4{}^2)[2 - \cos2\Theta_2 - \cos2(\Theta_1 + \Theta_2)] - (\sqrt{3}/2)(E_1E_2 + E_4E_5)[\cos2\Theta_2 - \cos2(\Theta_1 + \Theta_2)]\}, \quad (B1b)$$

$$F_{33}^{1}=\sum_n(\hbar N_n/3NM)\sum_\lambda \omega_{n\lambda}^{-1}(E_3^2+E_6^2)[3-\cos2\Theta_1-\cos2\Theta_2-\cos2(\Theta_1+\Theta_2)]\ , \tag{B1c}$$

$$F_{12}^{1}=F_{13}^{1}=F_{23}^{1}=0\ , \tag{B1d}$$

$$\begin{aligned}F_{11}^{8}=&\sum_n(\hbar N_n/3NM)\sum_\lambda \omega_{n\lambda}^{-1}(\tfrac{3}{2}[E_1^2+E_4^2+E_2^2+E_5^2]-\cos\Theta_3\{(E_1^2-E_4^2)\\&\times[\cos2\varphi+\tfrac{1}{4}\cos(\Theta_1+\varphi)+\tfrac{1}{4}\cos(\Theta_1-\varphi)]+\tfrac{3}{4}(E_2^2-E_5^2)[\cos(\Theta_1+\varphi)+\cos(\Theta_1-\varphi)]\\&-E_1E_4[2\sin2\varphi-\tfrac{1}{2}\sin(\Theta_1+\varphi)+\tfrac{1}{2}\sin(\Theta_1-\varphi)]+(\sqrt{3}/2)(E_1E_2-E_4E_5)[\cos(\Theta_1-\varphi)-\cos(\Theta_1+\varphi)]\\&-(\sqrt{3}/2)(E_1E_5+E_2E_4)[\sin(\Theta_1+\varphi)+\sin(\Theta_1-\varphi)]-\tfrac{3}{2}E_2E_5[\sin(\Theta_1-\varphi)-\sin(\Theta_1+\varphi)]\}\ ),\end{aligned} \tag{B2a}$$

$$\begin{aligned}F_{22}^{8}=&\sum_n(\hbar N_n/3NM)\sum_\lambda \omega_{n\lambda}^{-1}(\tfrac{3}{2}[E_1^2+E_4^2+E_2^2+E_5^2]-\cos\Theta_3\{(E_2^2-E_5^2)\\&\times[\cos2\varphi+\tfrac{1}{4}\cos(\Theta_1+\varphi)+\tfrac{1}{4}\cos(\Theta_1-\varphi)]+\tfrac{3}{4}(E_1^2-E_4^2)[\cos(\Theta_1+\varphi)+\cos(\Theta_1-\varphi)]\\&-E_2E_5[2\sin2\varphi-\tfrac{1}{2}\sin(\Theta_1+\varphi)+\tfrac{1}{2}\sin(\Theta_1-\varphi)]-(\sqrt{3}/2)(E_1E_2-E_4E_5)[\cos(\Theta_1-\varphi)-\cos(\Theta_1+\varphi)]\\&+(\sqrt{3}/2)(E_1E_5+E_2E_4)[\sin(\Theta_1+\varphi)+\sin(\Theta_1-\varphi)]-\tfrac{3}{2}E_1E_4[\sin(\Theta_1-\varphi)-\sin(\Theta_1+\varphi)]\}\ ),\end{aligned}$$

$$F_{33}^{8}=\sum_n(\hbar N_n/3NM)\sum_\lambda \omega_{n\lambda}^{-1}(3[E_3^2+E_6^2]-\cos\Theta_3\{(E_3^2-E_6^2) \tag{B2b}$$

$$\times[\cos2\varphi+\cos(\Theta_1+\varphi)+\cos(\Theta_1-\varphi)]-2E_3E_6[\sin2\varphi-\sin(\Theta_1+\varphi)+\sin(\Theta_1-\varphi)]\}\ ), \tag{B2c}$$

$$\begin{aligned}F_{23}^{8}=&-\sum_n(\hbar N_n/3NM)\sum_\lambda \omega_{n\lambda}^{-1}\sin\Theta_3\{(E_2E_3-E_5E_6)[\sin2\varphi+\tfrac{1}{2}\sin(\Theta_1+\varphi)-\tfrac{1}{2}\sin(\Theta_1-\varphi)]\\&-(E_3E_5+E_2E_6)[-\cos2\varphi+\tfrac{1}{2}\cos(\Theta_1+\varphi)+\tfrac{1}{2}\cos(\Theta_1-\varphi)]\\&+(\sqrt{3}/2)(E_1E_3-E_4E_6)[\sin(\Theta_1+\varphi)+\sin(\Theta_1-\varphi)]-(\sqrt{3}/2)(E_3E_4+E_1E_6)[\cos(\Theta_1+\varphi)-\cos(\Theta_1-\varphi)]\},\end{aligned} \tag{B2d}$$

and $F_{13}^{8}=F_{12}^{8}=0.$ (B2e)

The quantities Θ_1, Θ_2, and φ are defined in Appendix A. The parameter N_n represents the weight of the point n in the irreducible part of the first Brillouin zone, and E_i represents the ith component of the eigenvector $E(n;\lambda)$ which is real and has the dimension six. Details as to the values of N_n and the eigenvectors appear in Ref. 27.

APPENDIX C. THE COUPLING PARAMETER INTEGRALS

The expressions for the parameters α, β, γ, λ, μ, ν, and σ are obtained from (3.5), (3.16), and Table II:

$$\alpha=\tfrac{1}{2}\int[(x_1^2+x_2^2)f(x)+2g(x)]\,P^1(\vec{x}-\vec{R}^1)\,d\vec{x}\ , \tag{C1a}$$

$$\beta=\tfrac{1}{4}\int(x_1^2-x_2^2)f(x)\,P^1(\vec{x}-\vec{R}^1)\,d\vec{x}\ , \tag{C1b}$$

$$\lambda=\tfrac{1}{2}\int[(x_1^2+x_2^2)f(x)+2g(x)]\,P^8(\vec{x}-\vec{R}^8)\,d\vec{x}\ , \tag{C1c}$$

$$\mu=\tfrac{1}{4}\int(x_1^2-x_2^2)f(x)\,P^8(\vec{x}-\vec{R}^8)\,d\vec{x}\ , \tag{C1d}$$

$$\sigma=\tfrac{1}{2}\int x_2x_3f(x)\,P^8(\vec{x}-\vec{R}^8)\,d\vec{x}, \tag{C1e}$$

and

$$\nu=\int[x_3^2f(x)+g(x)]\,P^8(\vec{x}-\vec{R}^8)\,d\vec{x}\ , \tag{C1f}$$

where $x=|\vec{x}|$. The parameter γ is determined by using Eq. (3.5).

It is interesting to note that in the case of classical lattice dynamics we would have the following relations among the coupling parameters:

$$\alpha=2\beta+\gamma\ , \tag{C2a}$$

$$3^{1/2}c\mu=a\sigma\ , \tag{C2b}$$

and $$\lambda-\nu=(3c^2/a^2-2)\,\mu\ . \tag{C2c}$$

These conditions are invalidated by the quantum-mechanical averaging in the present case. For example, Eq. (C2a) is invalid because the x_2^2 term in (C1a) and (C1b) is nonzero.

*Work was performed in the Ames Laboratory of the U. S. Atomic Energy Commission; Contribution No. 2352.

†Present address: Department of Physics, Mankato State College, Mankato, Minnesota 56001.

[1]F. W. deWette and B. R. A. Nijboer, Phys. Letters 18, 19 (1965).
[2]N. Bernardes and H. Primakoff, Phys. Rev. 119, 968 (1960).
[3]N. Bernardes, Phys. Rev. 120, 1927 (1960).
[4]L. H. Nosanow and G. L. Shaw, Phys. Rev. 128, 546 (1962).
[5]D. Rosenwald, Phys. Rev. 154, 160 (1967).
[6]F. Iwamoto and H. Namaizawa, Prog. Theoret. Phys. Suppl. (Kyoto) Nos. 37 and 38, 234 (1966).
[7]E. M. Saunders, Phys. Rev. 126, 1724 (1962).
[8]R. L. Garwin and A. Landesman, Physics 2, 107 (1965).
[9]L. H. Nosanow, Phys. Rev. Letters 13, 270 (1964).
[10]L. H. Nosanow, in Proceedings of the Ninth International Conference on Low Temperature Physics, Columbus, Ohio, 1964, edited by J. G. Daunt, D. O. Edwards, F. J. Milford, M. Yaqub, (Plenum Press, New York, 1965), p. 277.
[11]L. H. Nosanow, Phys. Rev. 146, 120 (1966).
[12]J. H. Hetherington, W. M. Mullin and L. H. Nosanow, Phys. Rev. 154, 175 (1967).
[13]L. H. Nosanow and N. R. Werthamer, Phys. Rev. Letters 15, 618 (1965).
[14]F. W. deWette, L. H. Nosanow and N. R. Werthamer, Phys. Rev. 162, 824 (1967).
[15]T. R. Koehler, Phys. Rev. 139, A1097 (1965).
[16]T. R. Koehler, Phys. Rev. 141, 281 (1966).
[17]T. R. Koehler, Phys. Rev. 144, 789 (1966).
[18]T. R. Koehler, Phys. Rev. Letters 17, 89 (1966).
[19]T. R. Koehler, Phys. Rev. Letters 18, 654 (1967).
[20]See, for example, G. Leibfried and W. Ludwig, in Solid State Physics 12, 275 (1961).
[21]G. H. Begbie and M. Born, Proc. Roy. Soc. (London) A188, 179 (1947).
[22]See, for example, G. Leibfried and W. Ludwig, in Solid State Phys. 12, 298-301 (1961).
[23]L. J. Raubenheimer and G. Gilat, Phys. Rev. 157, 586 (1967).
[24]H. H. Sample and C. A. Swenson, Phys. Rev. 158, 188 (1967).
[25]E. C. Heltemes and C. A. Swenson, Phys. Rev. 128, 1512 (1962).
[26]J. P. Franck, Phys. Letters 11, 208 (1964).
[27]G. L. Morley, Ph. D. thesis, Iowa State University, 1967 (unpublished).

PHYSICAL REVIEW VOLUME 180, NUMBER 1 5 APRIL 1969

Evidence for Condensation of He^3 Atoms on the Surface of Bubbles in Liquid He^4 †

A. J. Dahm*

Physics Department, University of Pennsylvania, Philadelphia, Pennsylvania 19104

and

Physics Department, Case Western Reserve University, Cleveland, Ohio 44106

(Received 13 August 1968; revised manuscript received 23 December 1968)

A phenomenological model is presented to explain the reduction in the critical velocity for vortex-ring creation by negative ions in liquid helium when small concentrations of He^3 impurities are added. The model is based on the assumption that the surface state for a He^3 atom has a lower energy than the bulk state. This results in an enhanced concentration of He^3 atoms on the surface of the negative ions. This change in the surface affects the flow of liquid helium in the boundary layer around the ion. The effects of the difference in the surface of the positive and negative ions on the critical velocity is discussed in both the continuous and instantaneous vortex-ring creation models.

The creation of vortex rings in liquid helium was first discovered by Rayfield and Reif.[1] The critical velocity of the ion for vortex-ring creation has since been studied by Rayfield.[2,3] Recently Rayfield[4] reported a reduced critical velocity for vortex-ring formation by negative ions in the presence of He^3 impurities. The corresponding critical velocity for positive ions was found to be independent of He^3 concentration. The two species of ions are considered to differ drastically in structure. The commonly accepted models for the ions are as follows: The positive